Received: 18 February 2019 | Revised: 21 June 2019 | Accepted: 2 July 2019

DOI: 10.1002/aic.16721

PROCESS SYSTEMS ENGINEERING

AIChE JOURNAL

# A flexible air separation process: 2. Optimal operation using economic model predictive control

Adrian Caspari[2] | Christoph Offermanns[2] | Pascal Schäfer[2] | Adel Mhamdi[2] | Alexander Mitsos[1,2,3]

[1]JARA-ENERGY, 52056 Aachen, Germany

[2]AVT - Aachener Verfahrenstechnik, Process Systems Engineering, RWTH Aachen University, Aachen, Germany

[3]Energy Systems Engineering (IEK-10), Forschungszentrum Jülich, 52425 Jülich, Germany

**Correspondence**
Alexander Mitsos, AVT Process Systems Engineering, RWTH Aachen University, 52074 Aachen, Germany.
Email: amitsos@alum.mit.edu

## Abstract

The penetration of renewable electricity promises an economic advantage for flexible operation of energy-intense processes. One way to achieve flexible operation is economic model predictive control (eNMPC), where an economic dynamic optimization problem is directly solved at controller level taking into account a process model and operational constraints. We apply eNMPC in silico to an air separation process with an integrated liquefier and liquid-assist operation. We use a mechanistic dynamic model as both controller model and plant surrogate. We conduct a closed-loop case study over a time horizon of 2 days with historical electricity prices and input disturbances. We solve the dynamic optimization problems in DyOS. Compared to the optimal steady-state operation, the eNMPC operating strategy gives a significant improvement of 14%. We further show that the eNMPC enables economic improvements similar to an idealized quasistationary scheduling. While the eNMPC provides control profiles qualitatively similar to those obtained from deterministic global optimization of quasistationary scheduling, the eNMPC satisfies the product purity constraints all the time whereas the quasistationary scheduling sometimes fails to do so. The eNMPC applies local optimization methods and achieves profiles similar to the scheduling solved using deterministic global optimization methods over the complete closed-loop simulation time horizon.

**KEYWORDS**

air separation unit, demand side management, direct single-shooting, economic model predictive control, integrated liquefication cycle

## 1 | INTRODUCTION

The enhanced use of renewables, for example, onshore wind and photovoltaic, for electricity production results in fluctuating electricity prices.[1,2] Exploiting these fluctuations promises an economic advantage of flexibly operating electricity-intensive processes. There are two requirements: (a) a "flexible process", that is, a process with a wide operation range and without big losses of efficiency and (b) "flexible process operation", that is, exploiting the process flexibility in the operation. Thus, there is both economical and ecological incentive to take advantage of flexible process load adjustment as a reaction to changing market conditions. This is known as demand-side management (DSM).[3]

DSM has been applied to various process systems in the last decades, for example, by Ghobeity and Mitsos[4] and Brée et al.[5] Different concepts, recent advances and challenges of industrial DSM have been summarized by Zhang and Grossmann[6] and the rising need for flexible operation in context of the integration of renewable

energy sources and feedstocks has been explained in Reference 7. DSM with respect to the electricity market is promising especially when applied to electricity intensive process such as cryogenic air separation units (ASUs).[8,9] In the first part of this two-part work,[10] we proposed an air separation process with an integrated liquefication cycle and liquid assist operation. It produces liquid nitrogen and liquid oxygen and can be operated very flexibly with respect to the process power demand by varying the liquid production rates and the activity of the integrated liquefication cycle. We showed the wide operational range of the proposed process (i.e., that it is indeed a "flexible process") by solving several steady-state optimizations for varying liquid nitrogen and liquid oxygen production. Depending on the production rates, the process power demand can be varied by about 88% while satisfying the operational constraints including product purities, which can be exploited for DSM. For instance, the liquid production rate may be increased, leading to higher power demand, when the electricity price is high and decreased otherwise, while the oxygen production rate stays constant. Both, liquid and oxygen production rates may be varied according to fluctuating electricity prices while the product requirements in terms of amount and purity are satisfied. Therefore, in this article we focus on DSM of the proposed ASU with integrated liquefication cycle and liquid assist operation.

DSM of ASUs can be executed online, during operation, by integrating the process operation tasks of scheduling and control.[11-13] We use the terms of scheduling and control as defined, for example, by Reference 13, where control takes into account operational decisions on a time scale of minutes to hours and scheduling is used for operational decisions on a time scale of several hour up to days. The integration of scheduling and process control plays a crucial rule for the introduction of sustainable processes[7,12,14] and can be achieved either by accounting for the closed-loop system dynamics in the scheduling layer, for example,[15-21] or by applying economic model predictive control (eNMPC), also termed bottom-up strategy, for example, by Reference 13, where economic objectives are directly considered in the supervisory control layer, for example.[22,23]

In the first approach, based on scheduling with dynamic closed-loop approximations, an upper-layer scheduling optimization problem is solved to get setpoints. These setpoints are then passed to the control layer, for example, a model predictive tracking controller, which acts as process control. To achieve feasible setpoints, the process dynamics are considered in the scheduling layer by using a model which represents the closed-loop behavior of the process. This closed-loop model is obtained either by embedding the necessary optimality conditions of the process in closed-loop with a tracking controller[18-21] or by using a data-driven model to approximate closed-loop behavior.[15-17] The controller level is not altered by the top-down approaches. It is rather assumed that a suitable controller exists steering the process to the desired set-points. This scheduling with a closed-loop approximations approach has already been applied to ASUs. Baldea et al[13] presented an integrated scheduling and control framework. The closed-loop process dynamics are captured in the scheduling problem using linear low-dimensional time scale-bridging models and the actual controller has to adjust the process control variables to follow the setpoints resulting from the scheduling problem. Pattison et al[15-17] extended the framework presented by Baldea et al[13] to explicitly incorporate process inventories, such as storage tanks, into the scheduling and control problems and applied the framework closed-loop on a moving horizon. They applied their method to a single-product nitrogen ASU and achieved 2.7% savings in electricity cost over a time horizon of 3 days compared to constant production rate. Schäfer et al[24] compared NMPC to a linear model predictive control strategy in an application to the rectification section of an ASU. They applied NMPC to track set-points resulting from an offline dynamic optimization and showed that using NMPC offers advantages in the process agility compared to a linear model predictive tracking controller. While many authors[13,15-17] focused on the scheduling layer and its integration with the control layer, but not on the control layer itself, others[24] also studied different types of operation schemes for the control layer but does not consider the control action in the models for the scheduling layer. Jamaludin and Swartz[18,19] presented a dynamic real-time optimization strategy where the lower level MPC tracking controller is considered in the upper level by using a bilevel formulation where the lower level, that is, the MPC tracking problem, is substituted by its first order necessary optimality conditions. They thus presented a method belonging to the top-down approaches. Li and Swartz[20,21] transferred this approach to distributed control schemes.

An alternative to the scheduling approach with closed-loop models embedded is eNMPC, where the controller level itself accounts for the scheduling task, that is, an economic objective is used directly at the controller level instead of using a controller to track preoptimized profiles. eNMPC promises several advantages compared to the scheduling approach: The economic optimization problem is directly solved at the controller level with an embedded dynamic process model reflecting the process dynamics. Feasibility of predefined setpoints is thus not an issue in eNMPC. Therefore, a simple control architecture can be used and there is no need to map the economic goals and constraints to the actual control cost which would additionally require suitable controller tuning in the presence of more than one control variable and constraint. The exact constraints can directly be used on the controller level, so that no regulation of the constraints is needed. Closed-loop models or closed-loop approximations, for example,[15,17,18,20] are not required for eNMPC. This is an advantage, as the rigorous treatment of the closed-loop behavior by embedding the optimality conditions[18-21] leads to large set of constraints in the optimization problem that has to be solved online. On the other hand, data-driven closed-loop approximations[15-17] are limited because of the absence of extrapolability and the restriction to the current control praxis of the process. Additionally, there is a broad theoretical foundation on the performance, convergence, and stability of the eNMPC, for example.[25-27] On the other hand, eNMPC has the drawback that a model is required which adequately predicts the dynamic behavior of the process under consideration. In addition, eNMPC requires a dynamic optimization problem to be solved in real-time. However, eNMPC exploits the actual process dynamics directly on the controller layer. The process performance is, hence, not limited to an existing controller performance as in scheduling with dynamic closed-loop approximations. On the other hand, the

distinction of an upper layer economic problem and a tracking problem, as in References 15-17, assigns specific tasks to each operational layer without the requirement of weighting between economic and tracking objective. However, a tuning of weights would also be required at the tracking controller layer.

eNMPC has already been applied to ASUs. Huang et al[28] presented an eNMPC application to a single-product ASU producing gaseous nitrogen using an advanced-step NMPC formulation,[29,30] which is essentially a sensitivity based fast-update method. They used a collocation-based solution algorithm to solve the optimization problem. We recently applied a fast-update based eNMPC to an single-product ASU producing gaseous nitrogen that is then liquefied to be buffered in a storage tank.[31] Further we applied a fast-update based eNMPC to a large-scale multiproduct ASU using mechanistic models, showing that the method is real-time applicable.[32]

Neither the scheduling approach nor eNMPC has been applied to an ASU with integrated liquefier and liquid assist operation. Due to several internal recycles of the process, the large-scale nature of the process model, and the high flexibility potential shown in our first part,[10] the application of eNMPC to the process is a challenging and interesting task. Therefore our focus in this work is on eNMPC of the ASU we proposed in the first part with an integrated liquefication cycle and liquid assist operation.[10] Thus, we show how the process can be operated flexibly by directly exploiting the process dynamics on the controller level.

The remainder of the article is structured as follows. In the following section, we summarize the ASU and process model and the process control scheme. We explain the economic model predictive control approach and mathematical formulation afterwards. We then define the operational scenario and benchmark process operation schemes before describe the implementation. We show and discuss the results of the closed-loop simulation, and draw conclusions in the last two sections.

## 2 | PROCESS AND MODEL

We proposed an ASU for the production of liquid oxygen and liquid nitrogen (LOX and LIN, respectively).[10] Figure 1 gives the flowsheet of the process including the position of the control variables of the process. The process topology is based on a double column, an integrated liquefication cycle, and the nitrogen liquid assist operation.

A detailed process description is provided in the first part of our work[10] and is summarized in the following. Ambient air is compressed

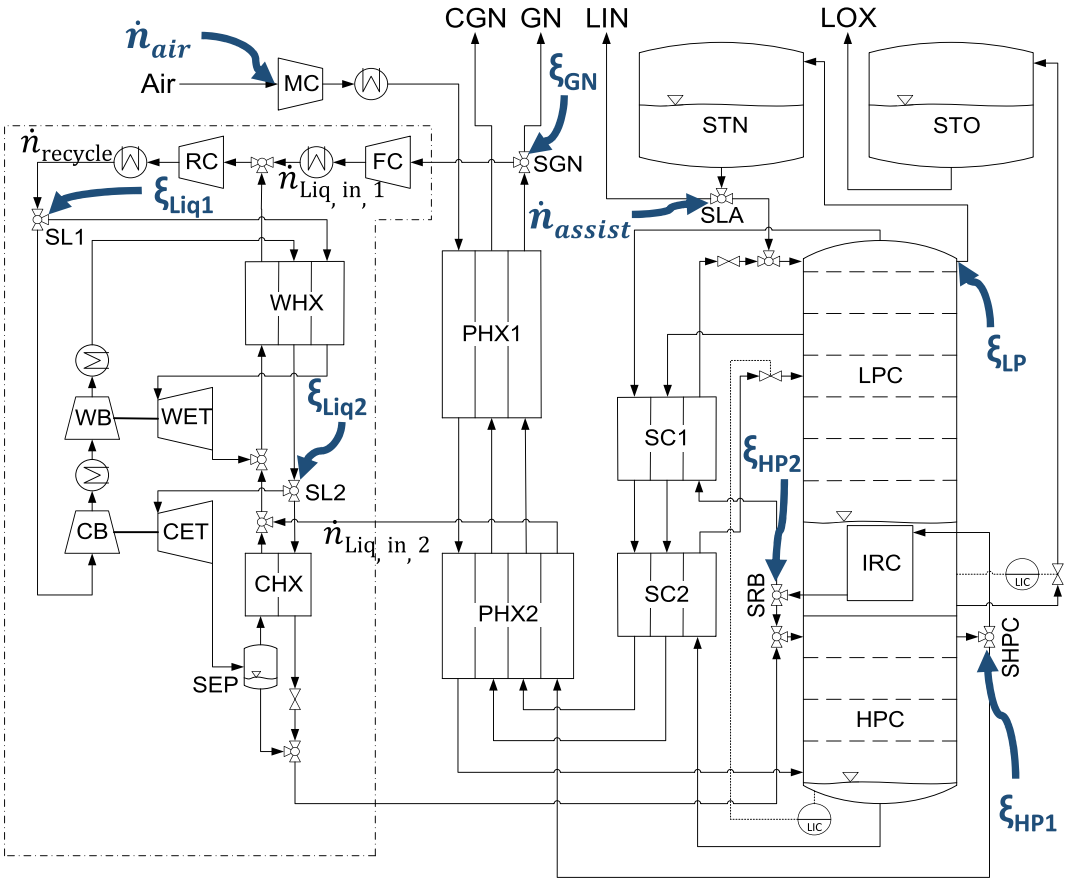


**FIGURE 1** Process flowsheet ASU with integrated nitrogen liquefication cycle (framed with dash-dotted line), liquid assist operation, and base-layer control (flow indicator controller with dashed lines). Cold/warm booster (CB and WB, respectively) and cold/warm expansion turbine (CET and WET, respectively) are energy integrated (dashed lines). The position of the control variables for the eNMPC case-study are indicated by the blue, bold symbols and arrows. ASU, air separation unit; eNMPC, economic model predictive control [Color figure can be viewed at wileyonlinelibrary.com]

to 6.5 bar in the main compressor (MC), cooled to 310 K, and is then chilled in the primary heat exchangers (PHX1 and PHX2) interacting countercurrently with the waste nitrogen waste streams (CGN and GN). The stream is then fed to the high pressure column (HPC). The HPC and the low pressure column (LPC) are energetically connected by an integrated reboiler-condenser (IRC). A nitrogen-rich stream is withdrawn from the HPC top, one part of it is sent to the IRC, the other part to the liquefication cycle. The IRC leaving stream is partially used as reflux for the HPC, as further feed stream for the liquefication cycle, and as feed stream to the LPC top, at 1.5 bar, after it is cooled in the subcooler (SC1). The oxygen-rich HPC bottom stream is chilled in the subcooler (SC2) and enters the LPC. The oxygen product is withdrawn from the LPC bottom, the nitrogen product is withdrawn form the LPC top. The product streams are fed to the nitrogen and oxygen storage tanks (STN and STO). Nitrogen product can be withdrawn from the process as product or sent back as reflux to the LPC, which is known as liquid-assist operation. A further top stream of the LPC leaves the process as gaseous nitrogen (GN), flowing through the SC1, SC2, PHX2, and PHX1. An additional withdrawal stream of the LPC leaves the process as crude gaseous nitrogen (CGN). A part of the GN is fed to the liquefication cycle, which provides the columns with reflux when the liquid assist operation is not active and additionally provides the process with cold liquid nitrogen by alternating compression, subsequent cooling to 310 K, and expansion. The feed compressor (FC) has an outlet pressure of 6.5 bar. The recycle compressor (RC) takes the recycle stream to 31 bar, the cold booster (CB) and warm booster (CB) to 55–75 bar, depending on the operational mode of the process. The streams are then expanded again in the warm expansion turbine (WET) and cold expansion turbine (CET) and sent to the separation (SEP). The liquefier streams are energetically integrated by the warm heat exchanger (WHX) and the cold heat exchanger (CHX). The liquid phase of the SEP is sent back to the HPC as reflux. The bottom holdups of the HPC and LPC are controlled using PI controller.

We use a detailed mechanistic process model which is also used as controller model. The model details can be found in the first part of our two-part article,[10] which we summarize in the following. Air is modeled as thermodynamic mixture of 78 mol% nitrogen, 21 mol% oxygen, and 1 mol% argon. We use Margules model[33] as activity model for the liquid phase and ideal gas for the vapor phase. We use an extended Antoine equation for the vapor pressures, equations from Reference 34 for ideal gas heat capacities, enthalpies, and entropies, and the Rackett equation[35] for the liquid densities. We calculate the enthalpies of vaporization using the DIPPR correlation of Aspen plus version 8.8 Plus. Compressors and turbines are modeled with constant isentropic efficiency. We model the heat exchanger as a one-dimensional spatially distributed system with finite differences and dynamic energy balances for the heat exchanger walls, steady-state equations for the fluids, and constant phase-dependent heat transfer coefficients. We model the rectification columns with equilibrium trays using the MESH equations with quasistationarity assumption for the specific enthalpy, a constant pressure drop, and a linear hydraulic correlation. The LPC has 65 and the HPC 40 equilibrium trays. CGN is withdrawn from the 12$^{th}$ stage of the LPC. We model the condenser as total condenser using steady-state equations, and the reboiler as equilibrium tray. We assume the tanks to be ideally thermally insulated.

The process model comprises 371 differential and 14,150 algebraic states after suitable discretization of the one-dimensional heat-exchanger models. The Modelica model is provided in the Supporting Information.

## 3 | MODEL PREDICTIVE CONTROL SCHEME

We apply the single-layer operation scheme depicted in Figure 2; an economic dynamic optimization problem (DO) is repeatedly solved online on a moving horizon using the current process states and a process model, cf., for example.[36] Using the scheme, we apply is an eNMPC without terminal constraints. A thorough theoretical analysis for the performance, convergence, and stability of eNMPC without terminal constraints for optimal periodic operation can be found in the work of Müller and Grüne.[27] In the following section, we describe the mathematical formulation of the economic DO problem solved at the controller layer.

### 3.1 | Mathematical formulation

The process model as described in detail in the first part [10] is a semi-explicit differential algebraic system with differential index of 1. Consequently, a DO problem on a finite time horizon $\mathcal{T} = [t_0, t_0 + t_c + t_p]$ of the following form is to be solved online:

$$\min_{\mathbf{u},\mathbf{x},\mathbf{y}} \Phi(\mathbf{u},\mathbf{x},\mathbf{y},\mathbf{p},\mathbf{d},\mathbf{q}) = \int_{t_0}^{t_0+t_c+t_p} L(\mathbf{x}(t),\mathbf{y}(t),\mathbf{u}(t),\mathbf{p}(t),\mathbf{d}(t))dt + \sum_{i=1}^{n_u} q_i \sum_{j=1}^{n_{c,i}-1} \left(u_{i,j+1} - u_{i,j}\right)^2 \tag{1a}$$

$$s.t. \mathbf{M}\dot{\mathbf{x}}(t) = \mathbf{f}(\mathbf{x}(t),\mathbf{y}(t),\mathbf{u}(t),\mathbf{d}(t),\mathbf{p}(t)), \forall t \in \mathcal{T} \tag{1b}$$

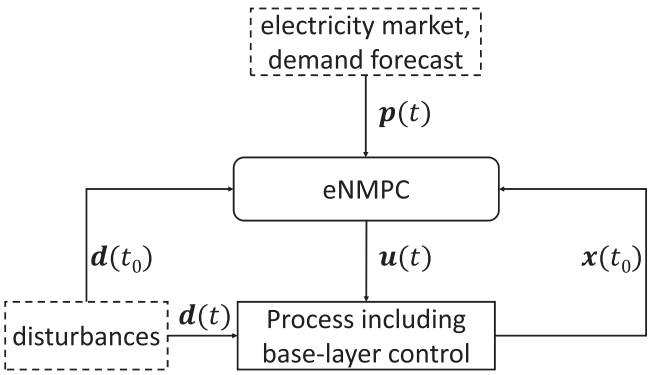


**FIGURE 2** Single-layer eNMPC scheme for flexible process operation. Electricity market and demand information are known over the control horizon. Disturbances are measured but unknown. They are assumed to be time-invariant over the control horizon. eNMPC, economic model predictive control

$$\mathbf{0} = \mathbf{g}(\mathbf{x}(t), \mathbf{y}(t), \mathbf{u}(t), \mathbf{d}(t), \mathbf{p}(t)), \forall t \in \mathcal{T} \tag{1c}$$

$$\mathbf{0} = \mathbf{h}(\mathbf{x}(t_0), \mathbf{y}(t_0), \mathbf{d}(t_0), \mathbf{p}(t_0)) \tag{1d}$$

$$\mathbf{0} \geq \mathbf{c}(\mathbf{x}(t), \mathbf{y}(t), \mathbf{u}(t), \mathbf{d}(t), \mathbf{p}(t)), t \in \mathcal{T} \tag{1e}$$

$$\boldsymbol{u}(t) = \boldsymbol{u}(t_c), t \in \mathcal{T} \mid t > t_c \tag{1f}$$

where $\mathbf{f}: \mathcal{X} \to \mathbb{R}^{n_x}$ and $\mathbf{g}: \mathcal{X} \to \mathbb{R}^{n_y}$ define the differential-algebraic system of index 1 with the constant and invertible matrix $\mathbf{M} \in \mathbb{R}^{n_x \times n_x}$, while $\mathbf{h}: \mathbb{R}^{n_x} \times \mathbb{R}^{n_y} \times \mathbb{R}^{n_u} \times \mathbb{R}^{n_p} \to \mathbb{R}^{n_x}$ indicates the initial conditions and $\mathbf{c}: \mathcal{X} \to \mathbb{R}^{n_c}$ are the constraints. We define $\mathcal{X} := \mathbb{R}^{n_x} \times \mathbb{R}^{n_y} \times \mathbb{R}^{n_u} \times \mathbb{R}^{n_p} \times \mathbb{R}^{n_d}$. $t_0 \in \mathbb{R}$ is the initial time. $t_c \in \mathbb{R}$ is the control horizon and $t_p \in \mathbb{R}$ is the prediction horizon. $\mathbf{u}: \mathcal{T} \to \mathbb{R}^{n_u}$ are the control variables, $\mathbf{x}: \mathcal{T} \to \mathbb{R}^{n_x}$ and $\mathbf{y}: \mathcal{T} \to \mathbb{R}^{n_y}$ are the state variables, $\mathbf{p}: \mathcal{T} \to \mathbb{R}^{n_p}$ are given parameter predefined variables, in this work the electricity prices and product demands, and $\mathbf{d}: \mathcal{T} \to \mathbb{R}^{n_d}$ are external disturbances, in this work the feed air temperature disturbances. The objective function to be minimized consists of an economic term and a penalty term: the economic term is the integrand of $L: \mathcal{X} \to \mathbb{R}$; the penalty term penalizes large control variable moves using the weights $\boldsymbol{q} \in \mathbb{R}^{n_u}$. The weights can be tuned so that the economic part of the objective function is greater than the penalty term. The control variables $u_i, i \in [1, n_u]$ are discretized using $n_{c,i}$ elements. We use direct single-shooting [37,38] to solve the optimization problems of the form (1). Using the penalty weights, we target smoother control variable profiles and facilitate the numerical integration of the process model during the optimization due to less fluctuating control variable profiles.

## 4 | OPERATIONAL SCENARIO

In this section, we explain the scenario for the closed-loop simulation, that is, how we define the parameter values $\mathbf{p}(t)$, the disturbance values $\mathbf{d}(t)$, and the initial condition (1d). After explaining the general definitions of the scenario and the eNMPC set-up, we describe the two benchmark operation schemes of an optimal constant operation and an optimal quasistationary scheduling operation used for comparison. Finally, we summarize the eNMPC and benchmark operations in Table 3.

We conduct simulations over a time horizon of 2 days. We assume a constant liquid product demand over the 2 days. We define a nominal product demand of 94 mol/s liquid oxygen and 58 mol/s liquid nitrogen. These values for the nominal production are the same as used in the first part of our paper.[10] All operation schemes as presented below have to satisfy this nominal product demand. We use historical electricity price data from the German day ahead market from 24th to 26th of February, 2018 shown in Figure 3a. The electricity prices have to be defined for more than 2 days as in each iteration the eNMPC uses the price information over the entire control and prediction horizon. As feed air, we use a mixture of 78 mol% of nitrogen, 21 mol% of oxygen, and 1 mol% of argon.

For the eNMPC operation and the optimal constant operation we assume the feed air temperature of the HX to be disturbed. The feed air temperature is shown in Figure 3b. The shown temperature steps may result from a pretreatment of the air using molecular sieves. A mole sieve regeneration switching from adsorption to desorption, takes place frequently, which trigger the temperature steps.[39] The disturbances are measured but the exact time-dependent profile is unknown by the eNMPC. The eNMPC assumes the disturbances to be constant for the whole control horizon.

### 4.1 | eNMPC process operation

The process behavior is simulated with the same model as the controller model, that is, there is no plant-model mismatch. We assume full state-feedback and neglect the time delay for the solution of the eNMPC optimization problem (1). For the optimization problem (1), we have to define the control and prediction horizon, the objective function, the operational constraints, control variables ranges and discretization, and the initial states for the DAE. For the eNMPC we use a sampling time of 15 min, a control horizon of 6 hr and a prediction horizon of 6 hr. Horizons of more than 12 hr might further improve the eNMPC performance, however, would also increase the computational time. We use the following economic term for the objective function (1a):

$$L(t) = p_{el}(t)(P_{MC}(t) + P_{RC}(t) + P_{FC}(t)),$$

where $p_{el}$ is the fluctuating electricity price. $P_{MC}$, $P_{RC}$, and $P_{FC}$ are the electricity demands of the compressors MC, RC, and FC.

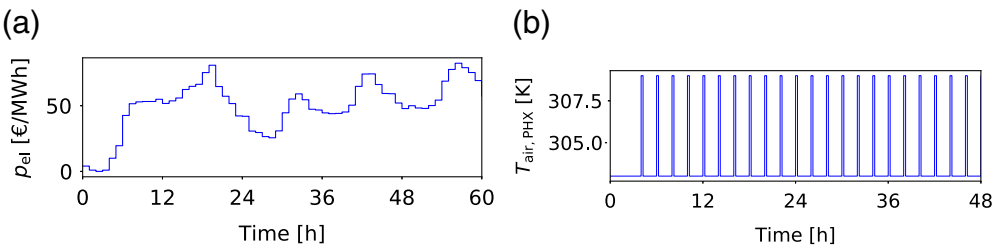


**FIGURE 3** Electricity price and disturbance profile for the case-study. (a) Electricity price of the day ahead auction for February 24, 25, and 26, 2018.[60] (b) Profile of the feed air stream temperature which is assumed to be disturbed due to molecular sieve switches in the air pretreatment [Color figure can be viewed at wileyonlinelibrary.com]

All constraints, control variables, and the operational cost term $L$ of the objective function are scaled to a range from 0 to 10. We reinitialize the objective function $\Phi$ (1) to zero before solving each eNMPC optimization problem to avoid scaling problems. The storage tank holdups are initialized at the beginning of the closed-loop simulation with an amount of product that corresponds to 1 day of nominal production. The STO is initialized with an amount that corresponds to 234 $m^3$ liquid oxygen, the STN is initialized with an amount corresponding to 177 $m^3$ liquid nitrogen. The eNMPC optimization problems apply the constraints summarized in Table 1. We constrain the product amount and purity. We use endpoint constraints to ensure that the STN and STO holdups are at their initial level from the beginning of the closed-loop simulation at the end of each prediction horizon. Thus, we enforce an average production of 94 mol/s liquid oxygen and 58 mol/s liquid nitrogen as required by definition of the scenario. We additionally constrain the maximum pressure of the warm booster WB outlet stream, which is the highest pressure in the whole process. We further constrain the vapor fraction of the cold expansion turbine CB outlet stream, to ensure that the stream is partially liquefied in the CB. The CHX outlet temperature difference $\Delta T_{CHX}$ and the IRC temperature difference $\Delta T_{CHX}$ are constrained to guarantee physical meaningful model behavior, that is, to be larger than a minimum value of 5 K. For the control variables we use an equidistant discretization of 30 min over the control horizon, that is, a discretization corresponding to two time of the eNMPC sampling time. For the constraints, we use an equidistant discretization of 5 min for the first hour and of 1 hr for the remaining hour of the control and prediction horizon. Thus, we reduce the risk of an intermediate constraint violation coming with a coarse discretization and on the other hand do not take the loss of high computational times coming with a fine constraint discretization; both function values and sensitivities have to be evaluated for each constraint at a discrete time point. By using a fine discretization at the first hour, we reduce intermediate constraint violation in the nearest future of the current eNMPC iteration starting point. We choose penalty weights for the control variables so that the penalty term for the stream variables is greater than the penalty term for the split factors and the complete penalty term is smaller than the economic term by one order of magnitude. We tune the penalty weights heuristically by performing several closed-loop simulations with different weights. The time-invariant initial values for the first eNMPC optimization of and the bounds on the control variables are summarized in Table 1. A warm-start strategy is implemented in which all subsequent eNMPC optimizations use the solution of the previous optimization as initial values for the control variables. As initial values for the control variables of the eNMPC, we use the result of the steady-state optimization and start the closed-loop simulation at the optimal steady-state for the given nominal production rate; the optimal steady-state is used as one benchmark operation and is explained in the next section.

**TABLE 1** Summary of the control variables and operational constraints

| Control | Lower bound | Upper bound | Penalty | Initial |
|---|---|---|---|---|
| $\dot{n}_{air}$ (mol/s) | 270 | 630 | 0.05 | 453.83 |
| $\dot{n}_{assist}$ (mol/s) | 0 | 150 | 0.05 | 1.096 |
| $\xi_{GNP}$ (–) | 0.001 | 0.999 | 0.1 | 0.64 |
| $\xi_{HP1}$ (–) | 0.5 | 0.98 | 0.1 | 0.85 |
| $\xi_{HP2}$ (–) | 0.2 | 0.3 | 0.1 | 0.3 |
| $\xi_{LP1}$ (–) | 0.001 | 1.0 | 0.1 | 0.28 |
| $\xi_{Liq1}$ (–) | 0.2 | 0.5 | 0.1 | 0.43 |
| $\xi_{Liq2}$ (–) | 0.7 | 0.9 | 0.1 | 0.83 |
| **Constraint** | **Lower bound** | **Upper bound** | **Type** | |
| $\varphi_{cet,\ out}$ | 0.85 | 0.98 | Path | |
| $p_{cet,\ out}$ (bar) | 55 | 75 | Path | |
| $\Delta T_{HX}$ (K) | 5 | - | Path | |
| $\Delta T_{IRC}$ (K) | 2 | - | Path | |
| $n_{STO}$ (mol) | 8,145,878.4 | 1e8 | Endpoint | |
| $n_{STN}$ (mol) | 4,997,305.152 | 1e8 | Endpoint | |
| $x_{LOX}$ (–) | 0.995 | 1.0 | Path | |
| $x_{LIN}$ (–) | 0.99995 | 1.0 | Path | |

*Note:* As initial values for the first eNMPC optimization, the solution of the steady-state optimization is used. $\dot{n}_{air}$ and $\dot{n}_{assist}$ are the feed air stream and the liquid assist stream, respectively. $\xi$ are split factors. $x_{LIN}$ and $x_{LOX}$ are the inlet stream purities of the LIN and LOX storage tank, STN and STO, respectively. $n_{STO}$ and $n_{STN}$ are the holdups of the LOX and LIN tank, STO and STN, respectively. $\phi_{cet,\ out}$ and $p_{cet,\ out}$ are the vapor fraction of the stream leaving the CET and the pressure of the stream entering the CET/leaving the WB, respectively.
Abbreviation: eNMPC, economic model predictive control.

## 4.2 | Benchmark I: optimal constant operation

We compare the eNMPC results with the optimal constant operation benchmark optimized with respect to the power usage and producing the same amount of liquid oxygen and nitrogen as the eNMPC during the 2-day time horizon of the case-study. The benchmark operation is taken from Reference 10. The steady-state optimization is performed subject to the same model minimizing

$$L = P_{MC} + P_{RC} + P_{FC},$$

with the same operational constraints as in the eNMPC. As a result, we obtain time-invariant optimal control variable values which we use as a benchmark operation. The benchmark operation is an open-loop operation; the control variable values from the optimal steady-state are used as control variable values in the benchmark simulation, where disturbances are present. Details about the steady-state optimization can be found in Reference 10. As we perform a steady-state optimization, the result does not depend on a specific electricity price profile. As benchmark, we simulate the steady-state optimization result using the same electricity price profile as the other operational schemes, as shown in Figure 3a.

## 4.3 | Benchmark II: optimal quasistationary scheduling

We use an optimal quasistationary scheduling without the consideration of the process dynamics in the scheduling layer as additional

benchmark. For this purpose, we fit a bivariate polynomial to the optimal overall process power usage as a function of the LIN and LOX production rate based on the results of the steady-state optimizations presented in the first part of the two-part article.[10] We discretize the time horizon $\mathcal{T}$ using $N_s \in \mathbb{N}$ elements and assume piecewise constant LIN production rates and electricity prices in each discretization element. We use the same equidistant discretization over the 2 days time horizon as for the eNMPC, that is, $\Delta t_i = 15\,\text{min} \;\; \forall i \in [1, N_s]$ and $N_s = 192$. We use one constraint to guarantee the same minimum amount of LIN and LOX to be produced as used by the eNMPC case-study and by the benchmark operation. The minimum amount of LIN is $N_{\text{LIN, min}} = 58\,\text{mol/s} \cdot 48\,\text{hr} \cdot 3,600\,\text{s/hr} = 10{,}002{,}400\,\text{mol}$. The minimum amount of LOX is $N_{\text{LOX, min}} = 94\,\text{mol/s} \cdot 48\,\text{hr} \cdot 3,600\,\text{s/hr} = 16{,}243{,}200\,\text{mol}$. We then minimize the overall power usage subject to the minimum amount of liquid nitrogen and oxygen produced over the time horizon of 2 days. Thus, the optimal schedule has the same minimum amount of liquid nitrogen and oxygen produced during the time horizon as the eNMPC and the optimal constant benchmark operation. We use the following quasistationary scheduling problem formulation

$$\begin{aligned} \min_{\dot{\boldsymbol{n}}_{\text{LIN}} \in \mathbb{LIN}, \dot{\boldsymbol{n}}_{\text{LOX}} \in \mathbb{LOX}} \quad & \text{cost}(\dot{\boldsymbol{n}}_{\text{LIN}}, \dot{\boldsymbol{n}}_{\text{LOX}}) = \sum_{i \in [1, N_s]} P_{\text{total}}\left(\dot{n}_{\text{LIN},i}, \dot{n}_{\text{LOX},i}\right) \cdot p_{\text{el},i} \cdot \Delta t_i \\ & s.t. \sum_{i \in [1, N_s]} \dot{n}_{\text{LIN},i} \cdot \Delta t_i \geq N_{\text{LIN, min}} \\ & \sum_{i \in [1, N_s]} \dot{n}_{\text{LOX},i} \cdot \Delta t_i \geq N_{\text{LOX, min}}, \end{aligned} \tag{2}$$

where $P_{\text{total}} : \mathbb{R}^2 \rightarrow \mathbb{R}$ is the bivariate polynomial regressed on the total power usage data presented in our previous work.[10] $\dot{\boldsymbol{n}}_{\text{LIN}} \in \mathbb{R}^{N_s}$ and $\dot{\boldsymbol{n}}_{\text{LOX}} \in \mathbb{R}^{N_s}$ are the discretized LIN and LOX production rates. $\boldsymbol{p}_{\text{el}} \in \mathbb{R}^{N_s}$ are the discretized electricity prices. $\boldsymbol{\Delta t} \in \mathbb{R}^{N_s}$ are the durations of the discrete time intervals, determined by $\Delta t_i = \mathcal{T}_i^{\text{d}} - \mathcal{T}_{i-1}^{\text{d}}$, where $T^{\text{d}} \in \mathbb{R}^{N_s}$ is the vector of discrete time points. $\mathbb{LIN} = [-130, 150]^{N_s}\,\text{mol/s}$ are the minimum and maximum LIN production rate. $\mathbb{LOX} = [50, 130]^{N_s}\,\text{mol/s}$ are the minimum and maximum LOX production rate. The optimal scheduling problem (2) has 384 degrees of freedoms. The optimal quasistationary scheduling benchmark is solved offline and does not consider any disturbance.

From the solution of (2), we obtain an optimal quasistationary schedule, that is, profiles for the LIN and LOX production rates. Using the steady-state optimization results of our previous work,[10] we interpolate the control variable values as function of the LIN and LOX production rates using piecewise linear interpolation. We use the optimal schedule as solution of (2) and the interpolated control variable values to calculate the profiles of the control variables. We then implement these control variable profiles for a forward simulation of the dynamic process model under the presence of disturbances to study the reaction of the dynamic model to the resulting control variable profiles from the optimal quasistationary schedule.

## 5 | PERFORMANCE COMPARISON

We compare the quasistationary scheduling and eNMPC operation strategy to the constant operation benchmark. We use the following measure to compare the performance of the eNMPC, the constant operation benchmark, and the quasistationary scheduling benchmark:

$$\eta_i = 1 - \frac{c_{\text{el},i}/n_{\text{prod},i}}{c_{\text{el,cob}}/n_{\text{prod,cob}}}, i \in \{\text{cob}, \text{eNMPC}, \text{os}\} \tag{3}$$

where $c_{\text{el, co}}$, $c_{\text{el, eNMPC}}$, and $c_{\text{el, os}}$ are the operation cost for the 2 days of the simulation of the constant operation benchmark operation, the eNMPC operation, and the optimal quasistationary scheduling benchmark operation, respectively with

$$c_{\text{el},i} = \int_{t_0}^{t_{\text{end}}} p_{\text{el}}(t)\left(P_{\text{MC},i}(t) + P_{\text{RC},i}(t) + P_{\text{FC},i}(t)\right)dt, i \in \{\text{cob}, \text{eNMPC}, \text{os}\}$$

$P_{\text{MC}}$, $P_{\text{RC}}$, and $P_{\text{FC}}$ are the power usage of the MC, RC, and FC, respectively, resulting from the with the different process operation schemes. $p_{\text{el}}$ is the time-dependent electricity price. The amount of product is calculated using

$$n_{\text{prod},i} = \int_{t_0}^{t_{\text{end}}} \dot{n}_{\text{LOX},i}(t) + \dot{n}_{\text{LIN},i}(t)dt, i \in \{\text{cob}, \text{eNMPC}, \text{os}\}$$

where $\dot{n}_{\text{LOX}}$ and $\dot{n}_{\text{LIN}}$ are the molar flow rates withdrawn from the LOX and LIN storage tank, respectively, resulting from the with the different operation schemes.

By using (3) as ratio for the improvement of the relative operation cost, we take different product amounts into account for the economic evaluation of the eNMPC and the benchmark process operations.

## 6 | IMPLEMENTATION

We implement the process model in Modelica,[40] export it as FMU,[41] and use the FMU in the optimizations and simulations. We solve the eNMPC optimization problems (1) and the process simulations in our open-source optimization framework DyOS[42,43] for direct adaptive shooting.[44,45] The overall framework for the closed-loop simulation is implemented in Python[46] using DyOS via its Python interface. In DyOS, we use the SQP solver SNOPT version 7.2-4[47] and the DAE integrator NIXE including sensitivity integration.[48] A Windows 7 desktop computer equipped with an Intel Core(TM) i3-6100 processor running at 3.7 GHz and 8 GB RAM is used for the computations of this work. The options of the integrator NIXE and the NLP solver SNOPT used for direct single-shooting in DyOS for the solution of the eNMPC optimization problem are summarized in Table 2.

The polynomial regression of the power usage as function of the production rates for the ideal scheduling benchmark is done using the Python machine learning package scikit-learn.[49] SciPy[50] is used for the piecewise linear interpolation of the control variable profiles based on

the steady-state optimization data. Baron version 16.3.4[51] is used from GAMS version 24.7.1[52] as deterministic global NLP solver for the solution of the ideal scheduling problem (2) with the default options.

## 7 | RESULTS AND DISCUSSION

We present open- and closed-loop simulation results of the multiproduct ASU over a time horizon of 2 days in this section. We show the benchmark operation results before the eNMPC operation results, and discuss them afterwards.

### 7.1 | Benchmark I: optimal constant process operation

The trajectories of the optimal constant operation are shown by the dashed lines in the Figures 4–7. The operational cost of the benchmark operation for 2 days are about 31,000 € and the amount of liquid product is $26.5 \times 10^6$ mol (Table 3). Because of the constant operation, the slope of the operational cost profile (Figure 6g), is proportional to the electricity price profile (Figure 3a). We see that the highest contribution to the operational cost is the power usage of the RC followed by the demand of the MC (Figure 4). The FC has the lowest electricity demand (Figure 4). The high electricity demand of the RC is due to the high recycle stream (Figure 5g).

The control variable values (Figure 7), correspond to the solution of the steady-state optimization and are hence constant. They are all within their bounds. The liquid assist stream (Figure 7b), is close to its lower bound. We see that the steady-state benchmark operation satisfies the operational constraints (Figure 6). The WB outlet pressure is at its upper bound (Figure 6f). The CHX temperature difference (Figure 6h), is at its lower bound. The IRC temperature difference (Figure 6i), is apart from the lower bound. The tank profiles are shown in Figure 6b,d. We see that the tank levels are constant as enforced by definition of the benchmark operation.

**TABLE 2** Options for the integrator NIXE and the NLP solver SNOPT

| Option | Value |
|---|---|
| Integrator tolerances for NIXE | $1 \times 10^{-3}$ |
| Major SQP iterations limit of SNOPT | 25 |
| Major step limit of SNOPT | $1 \times 10^{-2}$ |
| Major optimality tolerance of SNOPT | $1 \times 10^{-2}$ |
| Major feasibility tolerance of SNOPT | $1 \times 10^{-2}$ |

*Note:* We use the default values for the options not listed in the table.

### 7.2 | Benchmark II: optimal quasistationary scheduling

The bivariate polynomial regression for the power usage of the process as function of the production rates resulting from the steady-state optimizations is shown in Appendix C. A bivariate polynomial of order 8 precisely describes the data. The resulting trajectory of the LIN and LOX

**TABLE 3** Summary and economic evaluation of benchmark and eNMPC operation

| | Constant operation | Ideal scheduling | eNMPC |
|---|---|---|---|
| **Objective** | Power usage | Operation cost | Operation cost |
| **Optimization type** | Steady-state optimization by terminal state dynamic optimization | Quasistationary global deterministic optimization | Dynamic optimization |
| **Time-variable production** | No | Yes | Yes |
| **Cost (€)** | 31,072 | 26,333 | 28,053 |
| **Product amount (mol)** | 26,480,512 | 26,493,961 | 27,786,682 |
| **Improvement $\eta$ (%)** | 0 | 15.3 | 13.96 |

*Note:* The economic improvement is calculated using (3).
Abbreviation: eNMPC, economic model predictive control.

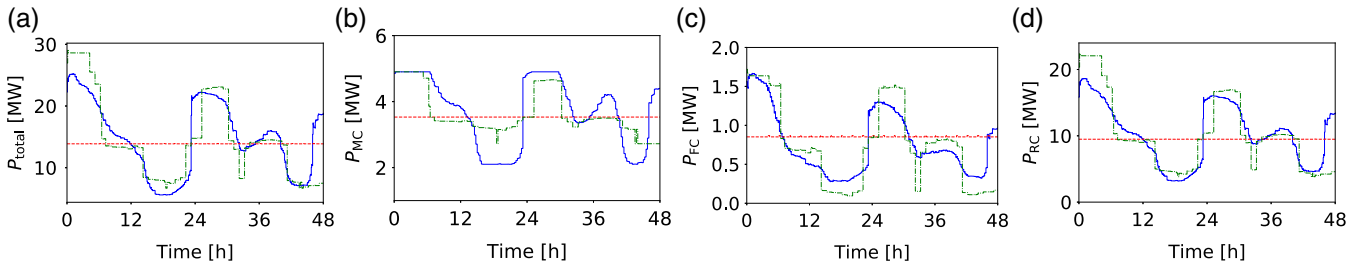


**FIGURE 4** Total power usage and single contributions to the electricity usage of the process. Optimal constant benchmark operation profiles dashed. eNMPC operation profiles solid. Quasistationary scheduling dash-dotted. (a) Total power usage. (b) Electricity usage of the main compressor MC. (c) Electricity usage of the integrated liquefier feed compressor FC. (d) Electricity demand of the integrated liquefier recycle compressor RC. eNMPC, economic model predictive control; FC, feed compressor; MC, main compressor [Color figure can be viewed at wileyonlinelibrary.com]

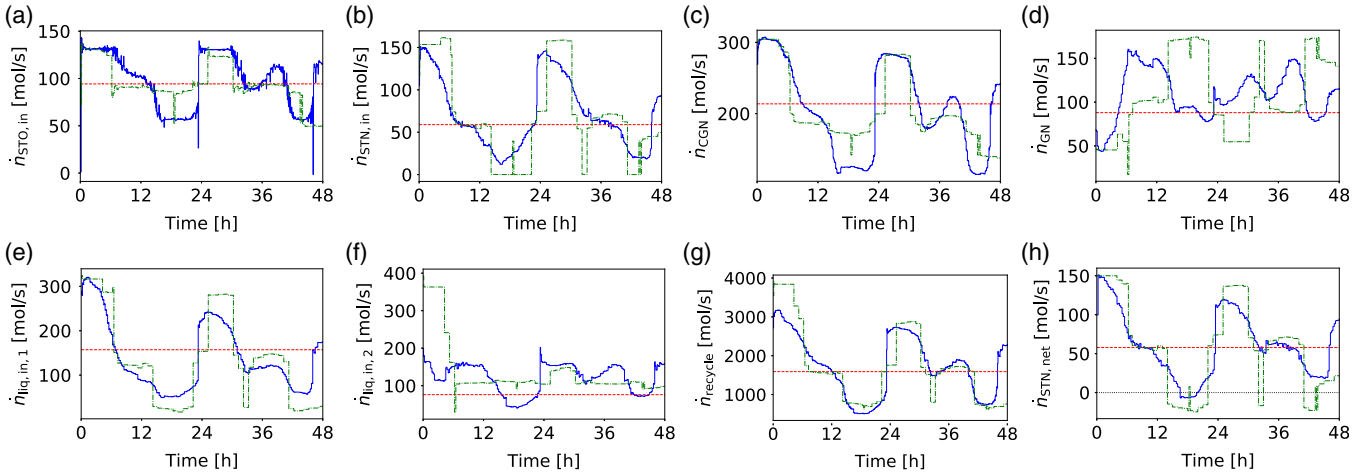


**FIGURE 5** Molar stream profiles. Optimal constant benchmark operation profiles dashed. eNMPC operation profiles solid. Quasistationary scheduling dash-dotted. Bounds dotted. (a) Inlet stream for LOX storage tank STO. (b) Inlet stream of LIN storage tank STN. (c) CNG waste stream. (d) GN waste stream. (e) Integrated liquefier inlet stream from splitter SCGN. (f) Integrated liquefier inlet stream from primary heat exchanger PHX2. (g) Integrated liquefier recycle stream. (h) STN net inlet stream as difference of STN feed stream and liquid assist stream. Zero marked with black, dotted line. eNMPC, economic model predictive control [Color figure can be viewed at wileyonlinelibrary.com]

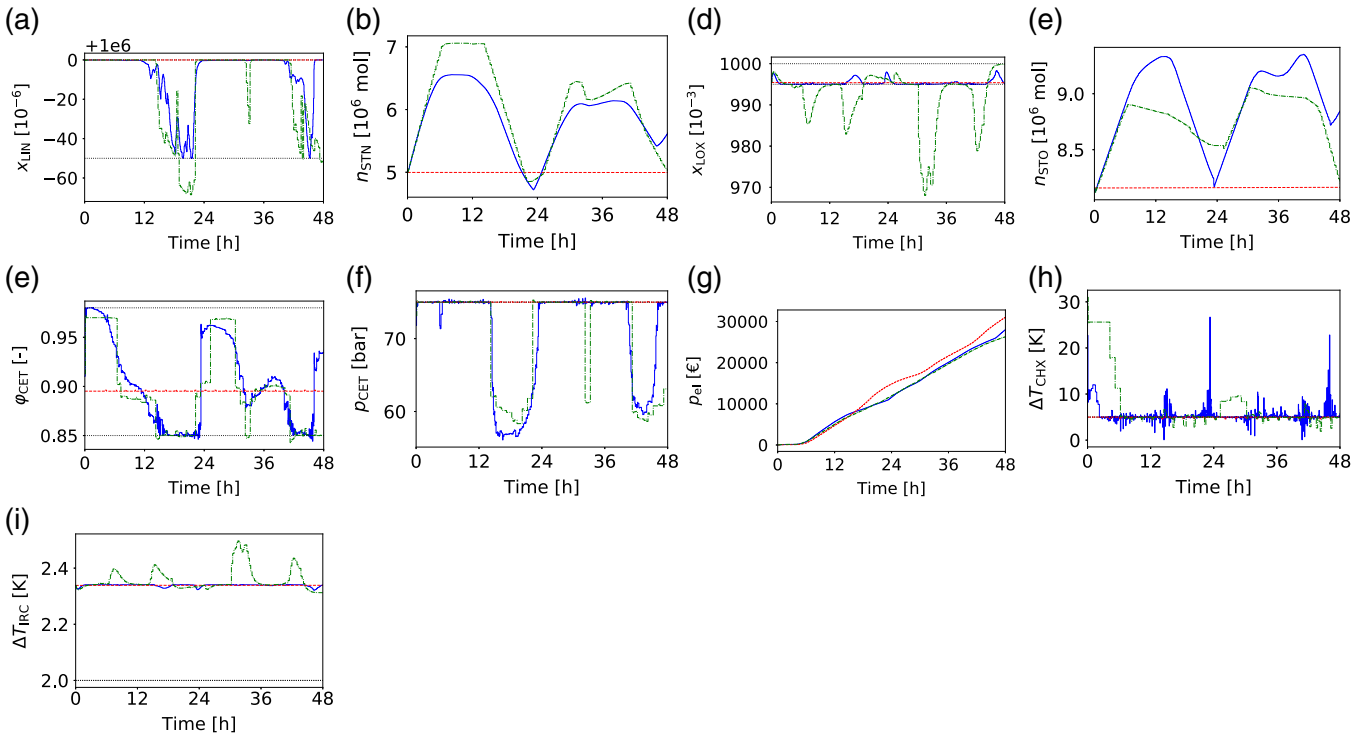


**FIGURE 6** State profiles. Optimal constant benchmark operation profiles dashed. eNMPC operation profiles solid. Quasistationary scheduling dash-dotted. Bounds dotted. (a) Purity of LIN product stream. (b) Molar holdup of LIN storage tank STN. (c) Purity of LOX product stream. (d) Molar holdup of LOX storage tank STO. (e) Liquid phase fraction of the stream leaving the cold expansion turbine CET. (f) Cold expansion turbine CET inlet pressure. (g) Process operation cost. (h) Cold heat exchanger CHE outlet temperature difference. (i) IRC temperature difference. eNMPC, economic model predictive control [Color figure can be viewed at wileyonlinelibrary.com]

production rate of the optimal scheduling operation are provided in Appendix C. The operation cost resulting from the scheduling operation is given in Table 3. The total CPU time for the global deterministic optimization of (2) is about 4 s. To see the reaction of the dynamic model to the quasistationary schedule, we interpolate the control variable profiles based on the steady-state optimization data and the LIN and LOX production rate profiles. Figures showing the interpolation of the control variables are provided in Appendix B. The resulting control profiles are shown with dash-dotted lines in Figure 7. We see that the control variable profiles reflect the electricity price fluctuations. Especially, the feed

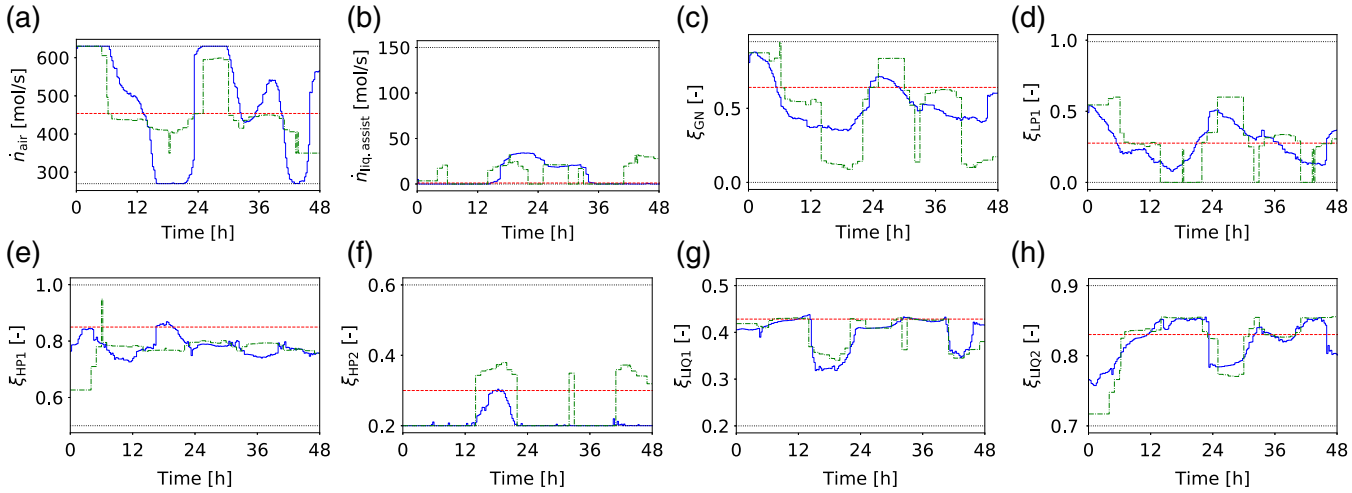


**FIGURE 7** Control variable profiles. Optimal constant benchmark operation profiles dashed. eNMPC operation profiles solid. Quasistationary scheduling dash-dotted. Bounds dotted. (a) Molar stream of main feed air. (b) Liquid assist operation flowrate. (c) Split factor of the splitter SCGN. Lower split factor increases the GN stream. (d) Split factor of the LP column. Higher split factor increases the liquid stream withdrawn from first stage of the column. (e) Split factor of the splitter SHPC. Higher split factor increases the stream sent to the integrated reboiler condenser RC. (f) Split factor of the splitter SRB. Higher split factor increases the reflux to the high pressure column HPC. (g) Split factor of the splitter SL1. Higher split factor increases the stream sent to the warm heat exchanger WHX. (h) Split factor of the splitter SL2. Higher split factor increases the stream sent to the cold expansion turbine CT. eNMPC, economic model predictive control [Color figure can be viewed at wileyonlinelibrary.com]

air stream is increased when the electricity price is high and decreased otherwise (Figure 7a). The liquid assist operation is active when the electricity price is low, so that more cooling is provided to the process, which in turn produces more liquid product that can then be used later. The liquid assist operation is active when the electricity price is high (Figure 7b) to provide reflux to the columns and cooling to the process when the liquefication cycle, fulfilling this tasks when the electricity price is low, is not active. The reaction of the dynamic process model to the controls resulting from the quasistationary scheduling are shown with dash-dotted lines in Figures 4–6. The power consumption profiles of the compressors, that is, the single contributor to the process power usage, reflect the electricity price fluctuations (Figure 4). The process power usage is high when the electricity price is low and vice versa (Figure 4a). The total power usage is mainly influenced by the RC (Figure 4d). The stream variables also reflect the electricity price fluctuations (Figure 5). The STN and STO feed streams are high when the electricity price is low and vice versa (Figure 5a,b). The liquid assist operation is active during low electricity price times (Figure 5h). The liquefication cycle activity is high when electricity price is low and vice versa (Figure 5e–g). The CGN waste stream is high and the GN waste stream is low when the electricity price is low (Figure 5c,d). We show selected state profiles of the optimal scheduling operation in Figure 6. We see that the STN and STO holdups clearly correspond to the electricity price profile; the tanks are loaded when the electricity price is low and unloaded otherwise (Figure 6b,d). The vapor fraction of the CET corresponds to the liquefication cycle activity (Figure 6e); the CET produces less liquid when the electricity price is high and more liquid otherwise. This is due to the increased CET flowrate when the liquefication cycle is active, and the fact that the CET inlet pressure is at its upper bound during this times. Increasing the amount of liquid is beneficial, however, it would require in increase in the CET inlet pressure. The CET inlet pressure is at the upper bound when the electricity price is low, to produce more liquid in the CET due to expansion from higher pressures (Figure 6f). This in turn provides more cooling to the process, so that more liquid is produced. The temperature differences in the CHX and IRC are always satisfied (Figure 6h,i). On the other hand, the optimal schedule violates the product purity constraints (Figure 6a,c), although all steady-state optimization problems used as basis for the optimal scheduling have been solved to convergence and were feasible. This shows that quasistationary scheduling is not enough in our case, where the process dynamics are slow and have to be taken into account for the operation. Clearly, more advanced scheduling approaches than the one used here or the combination of scheduling and tracking controllers could also be used for the process operation task which could increase the performance. However, while the combination of scheduling and tracking may improve the constraint violation it would also reduce the economic improvement obtained by the deterministic global solution of the scheduling problem.

### 7.3 | eNMPC process operation

The trajectories of the eNMPC operation are shown by the solid lines in the Figures 4–7. The electricity cost for the closed-loop operation for the 2 days of the simulation is 28,000 € and the amount of liquid product is $27.7 \times 10^6$ mol (Table 3). We see that, similar to the benchmark operation, the main contribution to the process power usage is due to the electricity demand of the RC, followed by the MC, and by the FC (Figure 4a). This is due to the high recycle stream (Figure 5g). The fluctuations of the power usage of the overall process (Figure 4a), results primarily from the fluctuations of the RC (Figure 4d). The cost

profile (Figure 6g), is the product of the electricity price (Figure 3a), and of the process power usage (Figure 4a). The slope of the cost profile is close to zero during the first time interval due to the low electricity price and significantly increases from about 6 to 12 hr, due to the high power usage. This is an intuitive behavior; the production rate is increased when the electricity price is low. The slope of the cost profile then decreases from 12 to about 18 hr, when the electricity price is high.

The control variables are within their bounds (Figure 7). The feed air streams varies in its full range, from the upper bound to the lower bound (Figure 7a). It is at its upper bound, when the electricity price is low, and decreases, when the electricity price increases. The liquid assist operation is active from about 14 hr to about 34 hr. It increases with increasing electricity prices and decreases otherwise. This is as expected as the RC stream of the liquefication cycle is reduced when the electricity price is high due to the high power usage of the RC. However, there is a positive tank feed stream at the same time when the liquid assist operation is active so that the effect of the liquid assist operation is lower then Figure 7b indicates. The net STN feed stream, that is, the difference of the feed stream and the liquid assist stream, is shown in Figure 5h. There is a negative stream, that is, liquid nitrogen is withdrawn from the STN, from about 16 to 20 hr, which is the time when the electricity price has is high. Outside of this time frame, the net stream is always positive, such that the tank is loaded. From this observation, we conclude, that liquid assist operation is actually activated only in case of strong electricity price fluctuations when the liquefication cycle activity is reduced. The split factor $\xi_{HP2}$ (Figure 7f), is at the lower bound most of the time, except between about 12 and 20 hr, that is, when the electricity price has is highest peak. A higher split factor increases the reflux to the HP and reduces the feed stream from the IRC via SC1 to the LPC. All other control variable profiles vary within their bounds with fluctuations in similar accordance to the electricity prices fluctuations.

Figure 6 shows selected state variable profiles. The product purities are satisfied at all times (Figure 6a,c). The tank profiles (Figure 6b,d), are intuitive; the tanks are loaded, when the electricity price is low and unloaded otherwise. The vapor fraction decreases, when the electricity price increases and increases otherwise (Figure 6e), that is, the liquid fraction of the CET increases, when the electricity price increases, and is maximum, when the electricity price is maximum. The CET inlet pressure/WB outlet pressure is at the upper bound most of the time and is reduced, when the electricity price has high peaks (Figure 6f). The temperature difference of the CHX is at its lower bound most of the time (Figure 6h). The lower bound is violated sometimes. However, the temperature difference is always positive so that physical model behavior is ensured. For the guaranteed path-constraint satisfaction, methods like published by Fu et al[53] are available. The IRC temperature difference constraint (Figure 6i), is satisfied. The use of a physical model allows to draw conclusions about further process improvements; the relaxation of the constraints regarding the minimum temperature difference in the heat exchanger, liquid fraction in the cold expansion turbine, and the maximum warm booster pressure could further improve the process economics.

Figure 5 shows selected stream variable profiles. We see that the STN and STO are feed streams are high, when the electricity price is low and low otherwise (Figure 5a,b). LIN is withdrawn from the STN and recycled to the process by liquid assist operation when the electricity price is maximum (Figure 5h). The liquefication cycle activity is reduced when the electricity price increases and the activity is increased otherwise (Figure 5e,f). The recycle stream (Figure 5g), fluctuates according to the electricity price profile, as the stream directly corresponds to the RC power usage, which has the highest contribution among all compressors to the process power usage.

The average CPU time for the solution of the dynamic optimization problems of the eNMPC is 1,136 s, with a standard deviation of 673 s, a minimum CPU time of 356 s, and a maximum CPU time of 3,363 s. The CPU times imply that the method applied in this work is not yet real-time applicable. However, the CPU times can be drastically reduced by using model reduction[54-56] or by applying different control architectures, for example, a two-layer architecture[57] where fast dynamics are treated using a fast neighboring extremal controller at the first level. Also modifications on the algorithm and implementation, such as the use of parallel programming, for example,[58,59] can further reduce computational times.

## 7.4 | Comparison of process operation approaches

Comparing the eNMPC and the optimal constant process operation, we see that the eNMPC leads to an improvement in the specific operational cost of 13.96% (Table 3). The eNMPC operation produces more product and achieves, in addition, less operating cost. Due to the 12 hr control horizon, the eNMPC accounts for the electricity price fluctuations for the 48 hr in the closed-loop simulation time horizon. Thus, it is economically beneficial to overproduce liquid oxygen and nitrogen to be used later. From the cost profile (Figure 6g), we see that the eNMPC operation is more expensive until about 14 hr. Then, the two profiles intersect and the eNMPC is cheaper for the remainder of the time. If the profiles converge, the eNMPC operation becomes more expensive than the benchmark operation and cheaper, if the profiles diverge. The power usage and the contributions to the power usage of the eNMPC operation fluctuate around the benchmark operation (Figure 4a–d). The eNMPC power usage is higher than the optimal constant benchmark operation power usage, when the electricity price is low and lower otherwise.

Most control variables vary around the steady-state benchmark operation profiles, for example, Figure 7a. The split factors $\xi_{HP1}$ and $\xi_{HP2}$ do not vary around the steady-state benchmark operation profiles but reach levels different from the benchmark operation profiles. The tank profile differences illustrate the economic efficiency of the eNMPC operation as compared to the optimal constant benchmark operation (Figure 6b,d). The eNMPC operation tank profiles are higher most of the time. The waste streams $\dot{n}_{CGN}$ of the eNMPC operation varies around the corresponding benchmark operation profile (Figure 5c). The waste streams $\dot{n}_{GN}$ of the eNMPC operation is higher than benchmark operation profile most of the time (Figure 5d).

In addition, we compare the eNMPC operation to the optimal scheduling operation defined by (2). The optimal schedule operation has an improvement of 15.3% with respect to the constant production benchmark. The economic performance of the optimal scheduling is about 1.5% better than the eNMPC performance. There are strong similarities between the profiles of the optimal scheduling operation and the eNMPC operation in all profiles. Although the eNMPC considers a time horizon of only 12 hr and uses local optimization methods, the control variable profiles are very similar to the profiles obtained by the optimal scheduling, which in contrast considers the complete 2 days as time horizon and uses deterministic global optimization methods (Figure 7). The process power usage of the scheduling operation is higher than the eNMPC operation when the electricity price is low and vice versa (Figure 4a). The optimal scheduling operation uses the liquid assist operation more extensively than the eNMPC (Figure 5h). Furthermore, the liquefication cycle is operated more extensively by the scheduling operation (Figure 5e–g). The scheduling operation uses the STN more extensively and the STO more moderately than the eNMPC (Figure 6b,d). The electricity cost profiles of the optimal scheduling and the eNMPC are very close to each other (Figure 3a); the eNMPC is more expensive during the first 20 hr and from about 36 hr on. However, in contrast to the eNMPC, the optimal scheduling operation violates the product purity constraints and produces less LIN and LOX (Figure 6a–d). This may result from the fact that the scheduling problem is not executed on a moving horizon; it is just calculated offline and the dynamic process model is then simulated with the resulting control variable profiles in an open-loop. On the other hand, the scheduling problem was solved globally, whereas we have no guarantee that the eNMPC is solved globally. Deterministic global optimization is, however, currently not applicable for large-scale dynamic optimization problems. Further, the scheduling benchmark is based on steady-state optimizations and we know that, under certain assumptions, the optimal dynamic operations outperforms the best steady-state and even the best cyclic steady-state.[25,27] This makes it very difficult to analyze accurately where the differences in the performance of the optimal scheduling and the eNMPC result from.

In the scheduling approach we are restricted to interpolation and our results show that both scheduling and eNMPC use the full range of the control variables, so that increasing the control variable ranges would require to generate new steady-state optimization data and new surrogate models for optimization. This is a drawback of using a data-driven surrogate model.

## 8 | CONCLUSION

ASUs are electricity intensive processes and thus well-suited for demand side management by varying the process control variable profiles on a time scale of minutes to several hours. eNMPC integrates the operation layers of scheduling and control and can in turn be used to apply DSM measures online. We apply economic model predictive control without terminal constraints to a large-scale air separation unit with an integrated liquefication cycle and liquid assist operation that we presented in the first part of the article.

We use a mechanistic model of the process and formulate an economic model predictive control problem. To solve the resulting large-scale dynamic optimization problem, we use direct single-shooting. Using this approach, we perform a closed-loop in silico case-study over 2 days including fluctuating electricity price profiles and inlet air temperature disturbances.

The economic model predictive controller achieves an economic improvement of about 14% with respect to the optimal constant operation benchmark while satisfying tight product purity constraints. Additionally, the eNMPC operation performance is slightly worse than the optimal quasistationary scheduling operation, which has been solved using a global deterministic solver. The control variable profiles of the eNMPC operation and the scheduling operation are very similar. However, in contrast to the eNNPC operation, the optimal quasistationary scheduling operation violates the product purity constraints. While the optimal quasistationary scheduling operation can be use to estimate the benefit of flexible operation, eNMPC allows to actual control the process flexibly. Although the eNMPC optimizes on the shorter time horizon than the optimal scheduling and uses local instead of global optimization, it achieves nearly identical control variable profiles and performance. Further, eNMPC enables to use the actual dynamic process model to be optimized, instead of surrogates, and thus allows to consider the actual process dynamic and to access all process model variables as constraints. In combination with a mechanistic model, eNMPC thus enables to optimize the actual physical model with the ability to extrapolate. On the other hand, eNMPC requires the application of computationally intensive methods for dynamic optimization, which are currently restricted to methods for local optimization. The use of global deterministic methods is currently restricted to small systems. In addition, the eNMPC trajectories are already very close to the trajectories of the optimal schedule, although they have been solved using local optimization. We show that the flexible operation of air separation units with integrated liquefication cycle and liquid assist operation under today's electricity prices offers significant economic improvements. The savings with respect to the constant operation result are primarily due to the flexible operation of the liquefier recycle compressor. The CPU times for solving the controller problem do not yet allow the method to be real-time applicable. The CPU time depends on the control and prediction horizon of the eNMPC, and on the discretization of the path constraints and control variables. We use a coarse discretization for the control variables during the control horizon to reduce the CPU times for the solution of the eNMPC problems and a shorter sampling time to increase the control variable flexibility and reduce the controller reaction time. Despite the horizon length of 12 hr for the control and prediction horizon, we obtain profiles which clearly reflect the electricity price of the day ahead market with its daily fluctuations. Furthermore, the control variable profiles of the eNMPC admits strong similarities with the scheduling operation although the latter considers the complete time horizon of 2 days, whereas the eNMPC considers a 12 hr horizon.

Further work should focus on reducing the computational demand for solving the eNMPC problem, for example, using SQP method with exact Hessians, control architectures with neighboring extremal fast-updates, model reduction techniques, and improvements of the algorithm and the implementation. The use of reduced models will introduce plant model mismatch, so that further work has to apply state estimation techniques, which may lead to further computational delay and uncertainties regarding the initial state. In addition, different electricity price scenarios can be used in future works to assess, when the liquefication cycle will be used more extensively. Further work should additionally integrate the eNMPC framework with a planning layer to provide optimal production rates for nitrogen and oxygen product to achieve a flexible production with respect to several days up to months. A detailed comparison of optimal scheduling with lower level tracking controller and eNMPC, that is, top-down with bottom-up approach is additionally left for future work. Finally, there are no rigorous tuning criteria for economic model predictive control, which would be a great enrichment and challenging work for the future.

## ACKNOWLEDGMENTS

The authors gratefully acknowledge the financial support of the Kopernikus project SynErgie by the Federal Ministry of Education and Research (BMBF) and the project supervision by the project management organization Projektträger Jülich (PtJ). The authors thank Anna-Maria Ecker, Andreas Peschel, Florian Schliebitz, and Gerhard Zapp from Linde AG, Johannes Faust, Falco C. Jung, and Yannic Vaupel from AVT.SVT, RWTH Aachen for fruitful discussions.

## ORCID

*Adrian Caspari* https://orcid.org/0000-0002-8521-4707
*Adel Mhamdi* https://orcid.org/0000-0003-0192-0864
*Alexander Mitsos* https://orcid.org/0000-0003-0335-6566

## REFERENCES

1. BDEW. https://www.bdew.de/presse/presseinformationen/erneuerbare-decken-38-prozent-des-stromverbrauchs/. Accessed 2018.
2. Agora. https://www.agora-energiewende.de/service/agorameter/chart/power_generation/12.11.2018/15.11.2018/. Accessed 2018.
3. Daryanian B, Bohn RE, Tabors RD. Optimal demand-side response to electricity spot prices for storage-type customers. *IEEE Power Eng Rev*. 1989;9:36-36.
4. Ghobeity A, Mitsos A. Optimal time-dependent operation of seawater reverse osmosis. *Desalination*. 2010;263:76-88.
5. Brée LC, Perrey K, Bulan A, Mitsos A. Demand side management and operational mode switching in chlorine production. *AIChE J*. 2018;65:e16352.
6. Zhang Q, Grossmann IE. Planning and scheduling for industrial demand side management: advances and challenges. In: Mariano M, ed. *Alternative Energy Sources and Technologies: Process Design and Operation*. Cham, Switzerland: Springer International Publishing; 2016:383-414.
7. Mitsos A, Asprion N, Floudas CA, et al. Challenges in process optimization for new feedstocks and energy sources. *Comput Chem Eng*. 2018;113:209-221.
8. Mitra S, Grossmann IE, Pinto JM, Arora N. Optimal production planning under time-sensitive electricity prices for continuous power-intensive processes. *Comput Chem Eng*. 2012;38:171-184.
9. Zhang Q, Grossmann IE, Heuberger CF, Sundaramoorthy A, Pinto JM. Air separation with cryogenic energy storage: optimal scheduling considering electric energy and reserve markets. *AIChE J*. 2015;61:1547-1558.
10. Caspari A, Offermanns C, Schäfer P, Mhamdi A, Mitsos A. A flexible air separation process: 1. Design and steady-state optimizations. *AIChE J*. 2019. https://doi.org/10.1002/aic.16705.
11. Harjunkoski I, Nyström R, Horch A. Integration of scheduling and control—theory or practice? *Comput Chem Eng*. 2009;33:1909-1918.
12. Baldea M, Harjunkoski I. Integrated production scheduling and process control: a systematic review. *Comput Chem Eng*. 2014;71:377-390.
13. Baldea M, Du J, Park J, Harjunkoski I. Integrated production scheduling and model predictive control of continuous processes. *AIChE J*. 2015;61:4179-4190.
14. Daoutidis P, Zachar M, Jogwar SS. Sustainability and process control: a survey and perspective. *J Process Control*. 2016;44:184-206.
15. Pattison RC, Touretzky CR, Johansson T, Harjunkoski I, Baldea M. Optimal process operations in fast-changing electricity markets: framework for scheduling with low-order dynamic models and an air separation application. *Ind Eng Chem Res*. 2016;55:4562-4584.
16. Pattison R, Touretzky CR, Johansson T, Baldea M, Harjunkoski I. Moving horizon scheduling of an air separation unit under fast-changing energy prices. *IFAC-PapersOnLine*. 2016;49:681-686.
17. Pattison RC, Touretzky CR, Harjunkoski I, Baldea M. Moving horizon closed-loop production scheduling using dynamic process models. *AIChE J*. 2017;63:639-651.
18. Jamaludin MZ, Swartz CLE. Closed-loop formulation for nonlinear dynamic real-time optimization. *IFAC-PapersOnLine*. 2016;49:406-411.
19. Jamaludin MZ, Swartz CLE. Approximation of closed-loop prediction for dynamic real-time optimization calculations. *Comput Chem Eng*. 2017;103:23-38.
20. Hao L, Swartz CLE. Approximation techniques for dynamic real-time optimization (DRTO) of distributed MPC systems. *Comput Chem Eng*. 2018;118:195-209.
21. Li H, Swartz CLE. Dynamic real-time optimization of distributed MPC systems using rigorous closed-loop prediction. *Comput Chem Eng*. 2018;122:356-371.
22. Engell S. Feedback control for optimal process operation. *J Process Control*. 2007;17:203-219.
23. Amrit R, Rawlings JB, Biegler LT. Optimizing process economics online using model predictive control. *Comput Chem Eng*. 2013;58:334-343.
24. Schäfer P, Bering LF, Caspari A, Mhamdi A, Mitsos A. Nonlinear dynamic optimization for improved load-shifting agility of cryogenic air separation plants. 13th International Symposium on Process Systems Engineering (PSE 2018); July 1–5, 2018; San Diego; 2018;547-552.
25. Angeli D, Amrit R, Rawlings JB. On average performance and stability of economic model predictive control. *IEEE Trans Automat Contr*. 2012;57:1615-1626.
26. Faulwasser T, Korda M, Jones CN, Bonvin D. Turnpike and dissipativity properties in dynamic real-time optimization and economic MPC. 53rd IEEE Conference on Decision and Control; December 15–17, 2014; Los Angeles, CA; 2014.
27. Müller MA, Grüne L. Economic model predictive control without terminal constraints for optimal periodic behavior. *Automatica*. 2016;70:128-139.

28. Huang R, Biegler LT. Economic NMPC for energy intensive applications with electricity price prediction. 11th International Symposium on Process Systems Engineering (PSE 2012), vol 31;15–19 July, 2012; Singapore; 2012:1612-1616.
29. Huang R, Zavala VM, Biegler LT. Advanced step nonlinear model predictive control for air separation units. *J Process Control*. 2009;19:678-685.
30. Zavala VM, Biegler LT. The advanced-step NMPC controller: optimality, stability and robustness. *Automatica*. 2009;45:86-93.
31. Caspari A, Faust JMM, Schäfer P, Mhamdi A, Mitsos A. Economic nonlinear model predictive control for flexible operation of air separation units. *IFAC-PapersOnLine*. 2018;51:295-300.
32. Caspari A, Perez Y Martin, Offermanns C, Schäfer P, Ecker A-M, Peschel A, Schliebitz F, Zapp G, Mhamdi A, Mitsos A. Economic nonlinear model predictive control of multi-product air separation processes. Computer-Aided Chemical Engineering; 2019;46.
33. Harmens A. Vapour-liquid equilibrium N2-Ar-O2 for lower argon concentrations. *Cryogenics*. 1970;10:406-409.
34. Aly FA, Lee LL. Self-consistent equations for calculating the ideal gas heat capacity, enthalpy, and entropy. *Fluid Phase Equilib*. 1981;6:169-179.
35. Green DW, Perry RH. *Perry's Chemical Engineers' Handbook*. New York City: McGraw-Hill Education Ltd. 2008:45–4393.
36. Binder T, Blank L, Bock HG, et al. Introduction to model based optimization of chemical processes on moving horizons. In: Grötschel M, Krumpke SO, Rambau J, eds. *Online Optimization of Large Scale Systems*. Berlin Heidelberg: Springer; 2001:295-339.
37. Brusch RG, Schapelle RH. Solution of highly constrained optimal control problems using nonlinear programing. *AIAA J*. 1973;11:135-136.
38. Sargent RWH, Sullivan GR. The development of an efficient optimal control package. In: Stoer J, ed. *Optimization Techniques*. Berlin Heidelberg: Springer; 1978:158-168.
39. Kerry FG. *Industrial Gas Handbook: Gas Separation and Purification*. Boca Raton: CRC Press; 2007.
40. Modelica. https://www.modelica.org/. Accessed 2018.
41. Functional Mock-Up Interface for Model Exchange and Co-Simulation. http://fmi-standard.org. Accessed 2018.
42. RWTH Aachen University, Aachener Verfahrenstechnik - Process Systems Engineering (AVT.SVT). DyOS- Dynamic Optimization Software. http://permalink.avt.rwthaachen.de/?id=295232. Accessed 2018.
43. Caspari A, Faust J M M, Jung F, Kappatou C, Sass S, Vaupel Y, Hannesmann-Tamás R, Mhamdi A, Mitsos A. DyOS - a framework for optimization of large-scale differential algebraic equation systems. Computer-Aided Chemical Engineering; 2019;46.
44. Schlegel M, Marquardt W, Ehrig R, Nowak U. Sensitivity analysis of linearly-implicit differential–algebraic systems by one-step extrapolation. *Appl Numer Math*. 2004;48:83-102.
45. Assassa F, Marquardt W. Dynamic optimization using adaptive direct multiple shooting. *Comput Chem Eng*. 2014;60:242-259.
46. Python. https://www.python.org/. Accessed 2018.
47. Philip EG, Murray W, Saunders MA. SNOPT: an SQP algorithm for large-scale constrained optimization. *SIAM Rev*. 2005;47:99-131.
48. Hannemann-Tamás R, Marquardt W, Naumann U, Gendler B. Discrete first- and second-order adjoints and automatic differentiation for the sensitivity analysis of dynamic models. *Procedia Comput Sci*. 2010;1:297-305.
49. scikit-learn. https://scikit-learn.org/stable/. Accessed 2019.
50. SciPy. https://www.scipy.org/. Accessed 2019.
51. Sahinidis NV. BARON: a general purpose global optimization software package. *J Glob Optim*. 1996;8:201-205.
52. GAMS. https://www.gams.com/. Accessed 2019.
53. Fu J, Faust JMM, Chachuat B, Mitsos A. Local optimization of dynamic programs with guaranteed satisfaction of path constraints. *Automatica*. 2015;62:184-192.
54. Marquardt W. Nonlinear model reduction for optimization based control of transient chemical processes. Chemical Process Control VI; Tucson Arizona; 2001;12-42.
55. Kienle A. Low-order dynamic models for ideal multicomponent distillation processes using nonlinear wave propagation theory. *Chem Eng Sci*. 2000;55:1817-1828.
56. Schäfer P, Caspari A, Kleinhans K, Mhamdi A, Mitsos A. Reduced dynamic modeling approach for rectification columns based on compartmentalization and artificial neural networks. *AIChE J*. 2019;65:e16568.
57. Würth L, Hannemann-Tamás R, Marquardt W. A two-layer architecture for economically optimal process control and operation. *J Process Control*. 2011;21:311-321.
58. Hartwich A, Stockmann K, Terboven C, Feuerriegel S, Marquardt W. Parallel sensitivity analysis for efficient large-scale dynamic optimization. *Optim Eng*. 2010;12:489-508.
59. Washington ID, Swartz CLE. Design under uncertainty using parallel multiperiod dynamic optimization. *AIChE J*. 2014;60:3151-3168.
60. Fraunhofer ISE. Bundesnetzagentur. SMARD Strommarktdaten. https://www.smard.de/home/marktdaten. Accessed 2018.


## SUPPORTING INFORMATION

Additional supporting information may be found online in the Supporting Information section at the end of this article.

**How to cite this article:** Caspari A, Offermanns C, Schäfer P, Mhamdi A, Mitsos A. A flexible air separation process: 2. Optimal operation using economic model predictive control. *AIChE J*. 2019;65:e16721. https://doi.org/10.1002/aic.16721